

LETTER TO THE EDITOR

Two distinct halo populations in the solar neighborhood [★] ^{★★}

Evidence from stellar abundance ratios and kinematics

P.E. Nissen¹ and W.J. Schuster²

¹ Department of Physics and Astronomy, University of Aarhus, DK-8000 Aarhus C, Denmark. e-mail: pen@phys.au.dk

² Observatorio Astronómico Nacional, Universidad Nacional Autónoma de México, Apartado Postal 877, C.P. 22800 Ensenada, B.C., México. e-mail: schuster@astrosen.unam.mx

Received 15 December 2009 / Accepted 18 February 2010

ABSTRACT

Aims. Precise abundance ratios are determined for 94 dwarf stars with $5200 < T_{\text{eff}} < 6300$ K, $-1.6 < [\text{Fe}/\text{H}] < -0.4$, and distances $D \lesssim 335$ pc. Most of them have halo kinematics, but 16 thick-disk stars are included.

Methods. Equivalent widths of atomic lines are measured from VLT/UVES and NOT/FIES spectra with resolutions $R \simeq 55\,000$ and $R \simeq 40\,000$, respectively. An LTE abundance analysis based on MARCS models is applied to derive precise differential abundance ratios of Na, Mg, Si, Ca, Ti, Cr, and Ni with respect to Fe.

Results. The halo stars fall into two populations, clearly separated in $[\alpha/\text{Fe}]$, where α refers to the average abundance of Mg, Si, Ca, and Ti. Differences in $[\text{Na}/\text{Fe}]$ and $[\text{Ni}/\text{Fe}]$ are also present with a remarkably clear correlation between these two abundance ratios.

Conclusions. The ‘high- α ’ stars may be ancient disk or bulge stars ‘heated’ to halo kinematics by merging satellite galaxies or they could have formed as the first stars during the collapse of a proto-Galactic gas cloud. The kinematics of the ‘low- α ’ stars suggest that they have been accreted from dwarf galaxies, and that some of them may originate from the ω Cen progenitor galaxy.

Key words. Stars: abundances – Stars: kinematics – Galaxy: halo – Galaxy: formation

1. Introduction

Studies of stellar populations are of high importance for understanding the formation and evolution of the Milky Way. In this context, it has been discussed whether the Galactic halo consists of more than one population. The monolithic collapse model of Eggen et al. (1962) corresponds to a single population, but from a study of globular clusters, Searle and Zinn (1978) suggested that the halo contains two populations: *i*) an inner, old, flattened population with a slight prograde rotation formed during a dissipative collapse, and *ii*) an outer, younger, spherical population accreted from dwarf galaxies. The presence of this dichotomy was supported by a study of $\sim 20\,000$ stars in the SDSS survey performed by Carollo et al. (2007).

Elemental abundances of stars in the solar neighborhood may provide additional information about the halo populations. In this context, the ratio $[\alpha/\text{Fe}]$, where α refers to the average abundance of Mg, Si, Ca, and Ti, is of particular interest. The α -elements are produced mainly during Type II supernovae (SNe) explosions on a short timescale ($\sim 10^7$ years), whereas iron is also produced by Type Ia SNe on a much longer timescale ($\sim 10^9$ years). Hence, $[\alpha/\text{Fe}]$ can

be used as a ‘clock’ to probe the star formation history of a Galactic component.

Several previous studies have focused on the possible differences in $[\alpha/\text{Fe}]$ for stars in the solar neighborhood. Fulbright (2002), Stephens & Boesgaard (2002), and Gratton et al. (2003) all find evidence that stars associated with the outer halo have lower $[\alpha/\text{Fe}]$ than stars connected to the inner halo. The differences in $[\alpha/\text{Fe}]$ found in these studies are, however, not larger than 0.1 dex, and it is unclear whether the distribution of $[\alpha/\text{Fe}]$ is continuous or bimodal. Nissen & Schuster (1997) achieved a higher precision measurement of $[\alpha/\text{Fe}]$ and found evidence of a bimodal distribution of $[\alpha/\text{Fe}]$ for 13 halo stars with $-1.3 < [\text{Fe}/\text{H}] < -0.4$, but a larger sample of these ‘metal-rich’ halo stars needs to be observed to confirm these findings and study possible correlations with kinematics. In this Letter, we present the first results of such a study.

2. Sample selection and observed spectra

Stars were selected from the Schuster et al. (2006) *uvby- β* catalogue of high-velocity and metal-poor stars. To ensure that a star has a high probability of belonging to the halo population, the total space velocity, V_{total} , with respect to the local standard of rest (LSR) was constrained to be larger than 180 km s^{-1} (Venn et al. 2004). Furthermore, the Strömberg indices ($b-y$), m_1 and c_1 were used to select dwarfs and subgiants with $5200 < T_{\text{eff}} < 6300$ K and $[\text{Fe}/\text{H}] \gtrsim -1.6$. This produced a list of about 200

[★] Based on observations made with the Nordic Optical Telescope on La Palma, and on data from the European Southern Observatory ESO/ST-ECF Science Archive Facility.

^{★★} Tables 3 and 4 are also available in electronic form at the CDS via anonymous ftp to cdsarc.u-strasbg.fr (130.79.128.5) or via <http://cdsweb.u-strasbg.fr/cgi-bin/qcat?J/A+A/>

stars, of which 37 have VLT/UVES spectra available in the ESO/ST-ECF Science Archive (Table 1). Furthermore, 16 stars with thick-disk kinematics and UVES spectra were included. In addition, 53 randomly selected stars were observed with the Fibre fed Echelle Spectrograph (FIES) at the Nordic Optical Telescope (NOT) (Table 2). Six were found to be double-lined spectroscopic binaries and excluded. All FIES stars and most of the UVES stars are brighter than $V = 11.1$, three having $V = 11.2$, 12.2, and 12.8. The average distance is 115 pc with $D_{\max} = 335$ pc.

The UVES spectra cover the spectral region 4800 - 6800 Å and have resolutions $R \simeq 55\,000$ and signal-to-noise ratios (S/N) from 250 to 500. The FIES spectra range from 4000 to 7000 Å, but only the 4700 - 6400 Å region was employed, with a resolution $R \simeq 40\,000$ and $S/N \simeq 140 - 200$. The majority of the UVES stars had reduced spectra available in the archive, but for stars observed with an image slicer, the raw data were reduced using the echelle package in IRAF. The FIES data were handled by FIES`tool`, a data reduction package developed by E. Stempels.

Equivalent widths (EWs) of 130 to 180 atomic lines were measured for each star. The large majority of the lines have EWs between 2 and 90 mÅ. For six stars, both UVES and FIES spectra are available. The average EW difference (FIES - UVES) is 0.6 mÅ with a rms deviation of 1.3 mÅ.

3. Stellar parameters and abundances

Element abundances are derived from EWs using the Uppsala EQWIDTH program together with model atmospheres interpolated from the new MARCS grid (Gustafsson et al. 2008). Two sets of models are available with different values of $[\alpha/Fe]$, which makes it possible to interpolate to a model having the same $[\alpha/Fe]$ as the star. Local thermodynamic equilibrium (LTE) is assumed in the line calculations, and line broadening caused by microturbulence, ξ_{turb} , and collisional damping is included.

The abundance analysis is performed differentially with respect to two bright thick-disk stars, HD 22879 and HD 76932. Their effective temperatures are determined from $(b-y)$ and $(V-K)$ using the calibrations of Ramírez & Meléndez (2005). Surface gravities are derived from Hipparcos parallaxes as described by Nissen et al. (2004), and chemical abundances from a differential analysis with respect to the Sun, using a subset of ~ 80 lines, which are relatively unblended in the solar flux spectrum of Kurucz et al. (1984). In an ‘inverted’ abundance analysis, the data from the star-Sun analysis are then used to determine gf -values for the whole set of ~ 180 lines. These gf -values are applied for the abundance analysis of all program stars.

We then determine T_{eff} so that the $[Fe/H]$ derived from the Fe I lines is independent of excitation potential. As the Fe I lines are also used to determine ξ_{turb} by minimizing the dependence of $[Fe/H]$ on EW, iteration is needed to obtain consistent values of T_{eff} and ξ_{turb} . We estimate a differential error of $\sigma(T_{\text{eff}}) = \pm 30$ K by comparing T_{eff} values derived from the Fe I excitation balance with those inferred from $(b-y)$ and $(V-K)$ colors for a subset of 44 nearby stars that appear to be unreddened according to the absence of interstellar NaD lines. The surface gravity is estimated by ensuring that Fe I and Fe II lines provide consistent Fe abundances. Comparison of these spectroscopic gravities with values determined from Hipparcos parallaxes

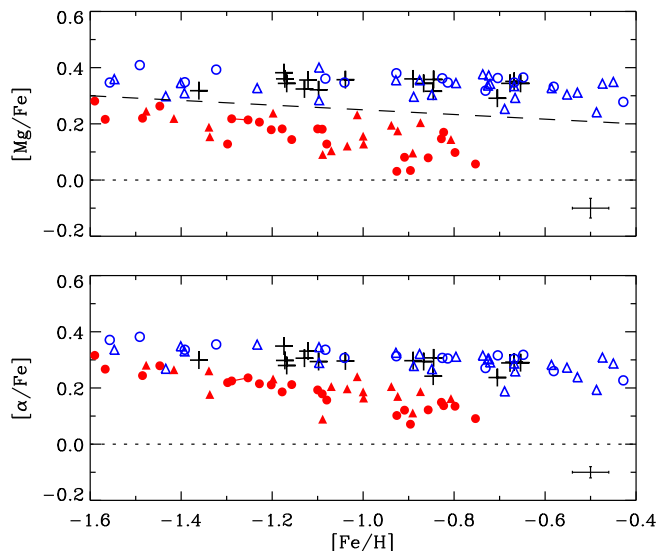


Fig. 1. $[Mg/Fe]$ and $[\alpha/Fe]$ versus $[Fe/H]$. Crosses refer to thick-disk stars and circles to halo stars observed with UVES. Triangles indicate halo stars with FIES spectra. Halo stars above the long-dashed line in the $[Mg/Fe]$ diagram are defined as belonging to the high- α population and are indicated by open (blue) symbols. The stars below the long-dashed line are defined to be low- α stars and are shown with filled (red) symbols. Based on $[Mg/Fe]$, this classification is maintained in all the following figures. The components of a visual binary star, G 112-43 and G 112-44, are connected by a straight line.

for the nearby stars shows that $\log g$ is determined differentially to a precision of 0.05 dex.

The derived abundance ratios of Na, Mg, Si, Ca, Ti, Cr, and Ni with respect to Fe are given in Tables 3 and 4. All abundance ratios are based on neutral lines. The numbers of the lines applied are Na I 2-5, Mg I 1-2, Si I 5-10, Ca I 6-9, Ti I 9-14, Cr I 4-7, Fe I 70-92, Fe II 14-16, and Ni I 20-27, where the first number refers to the most metal-poor stars, and the last to the most metal-rich.

The errors in the abundance ratios were estimated by comparing results obtained from UVES and FIES spectra for the six stars observed with both instruments (see Tables 3 and 4). The spectra of these stars have typical S/N , except HD 189558 that has an unusually high quality FIES spectrum ($S/N \simeq 350$). This comparison shows that differential values of $[Fe/H]$, $[Na/Fe]$, $[Mg/Fe]$, and $[Si/Fe]$ are determined to a $1-\sigma$ precision of 0.03 to 0.04 dex, whereas the precision of $[Ca/Fe]$, $[Ti/Fe]$, $[Cr/Fe]$, and $[\alpha/Fe]$ is about 0.02 dex. The error in $[Ni/Fe]$ is as small as 0.01 dex, because of the many Fe I and Ni I lines available. We note that errors in the abundance ratios caused by errors in T_{eff} and $\log g$ are small compared to errors induced by the EW measurements, because all ratios are derived from neutral atomic lines with similar sensitivity to T_{eff} and $\log g$.

Figure 1 shows $[Mg/Fe]$ and $[\alpha/Fe]$ as a function of $[Fe/H]$. We note that there are no systematic offsets between the UVES and the FIES data. The corresponding figure for $[Si/Fe]$, $[Ca/Fe]$, and $[Ti/Fe]$ is shown in the Online Section. As can be seen, the halo stars consist of two distinct populations, the ‘high- α ’ stars with a nearly constant $[\alpha/Fe]$ and the ‘low- α ’ stars with a declining $[\alpha/Fe]$ as a function of increasing metallicity. A classification into these two populations was performed on the basis of $[Mg/Fe]$. In

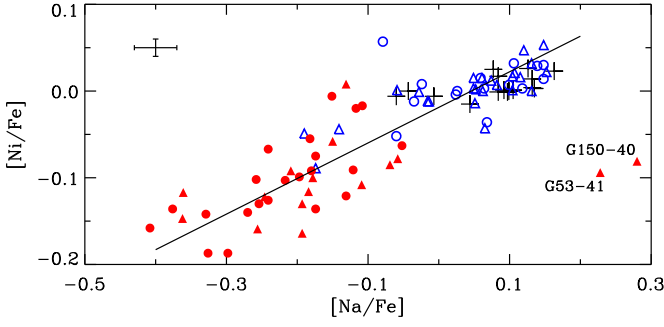


Fig. 2. $[\text{Ni}/\text{Fe}]$ versus $[\text{Na}/\text{Fe}]$ with the same symbols as in Fig. 1. The linear fit does not include the two Na-rich stars.

the range $-1.6 < [\text{Fe}/\text{H}] < -1.4$, the two populations tend to merge, and the classification is less clear. The high- α and low- α halo populations also separate well in $[\text{Na}/\text{Fe}]$ and $[\text{Ni}/\text{Fe}]$ with the exceptions of two Na-rich stars. The abundance differences can be seen directly from the observed spectra as shown in the Online Section.

The scatter in the abundance ratios for the high- α and thick-disk stars relative to the best-fit linear relations is 0.032 dex for $[\text{Mg}/\text{Fe}]$ and 0.030 dex for $[\alpha/\text{Fe}]$. This is similar to the estimated errors of the analysis. For the low- α stars, there are, however, abundance differences from the trends that cannot be explained by the errors alone, especially in the case of $[\text{Na}/\text{Fe}]$ and $[\text{Ni}/\text{Fe}]$. The clear correlation between these ratios (Fig. 2) confirms that cosmic variations in these ratios are present at a given $[\text{Fe}/\text{H}]$.

4. Kinematics

To calculate the stellar space velocities, we acquired proper motions from the Tycho-2 catalogue (Høg et al. 2000, 88 stars), the new reduction of the Hipparcos data (van Leeuwen 2007, 4 stars), and the revised NLTT (Salim & Gould 2003, 2 stars). Distances of stars were calculated from the parallaxes of van Leeuwen (2007), when the errors in these are less than 10%, and if not, from the photometric absolute magnitude calibration by Schuster et al. (2004, 2006). The radial velocities of the stars were derived from our own spectra and have errors of $\pm 0.3 \text{ km s}^{-1}$.

With these data as input, the formulae and matrix equations of Johnson & Soderblom (1987) were used to calculate the Galactic velocity components (U, V, W) and their errors. Correction for a solar motion of $(+7.5, +13.5, +6.8) \text{ km s}^{-1}$ with respect to the LSR was adopted from Francis & Anderson (2009). The resulting values of $U_{\text{LSR}}, V_{\text{LSR}}$, and W_{LSR} are given in Tables 3 and 4. The average errors of these velocities for the halo stars are $(\pm 12, \pm 16, \pm 9) \text{ km s}^{-1}$ with a major contribution from the error in the distances.

Figure 3 shows the Toomre diagram for the thick-disk and halo stars that could be clearly classified as belonging to either the high- α or the low- α population. Assuming Gaussian velocity distributions with canonical dispersions and asymmetric drifts for the thin-disk, thick-disk, and halo populations, stars with $V_{\text{total}} > 180 \text{ km s}^{-1}$ generally have a high probability of belonging to the halo population (Venn et al. 2004). If, on the other hand, the velocity distribution of the thick disk is non-Gaussian with an extended tail toward high velocities, as in the model of the Galactic disks by Schönrich & Binney (2009), then the high- α stars with

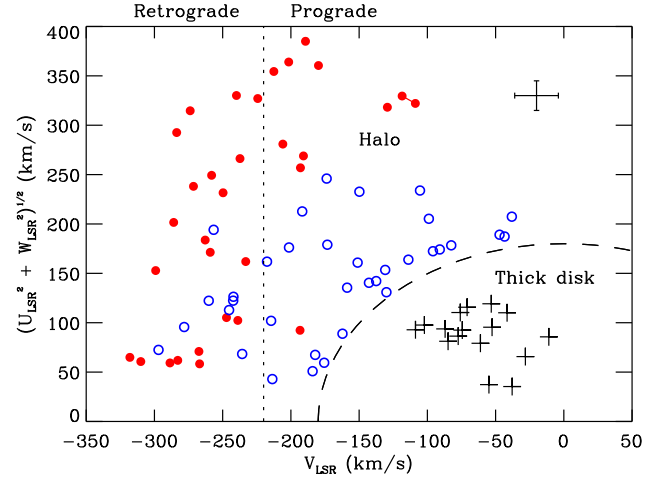


Fig. 3. Toomre diagram for stars with $[\text{Fe}/\text{H}] > -1.4$. High- α halo stars are shown with open (blue) circles, low- α halo stars with filled (red) circles, and thick-disk stars with crosses. The long-dashed line corresponds to $V_{\text{total}} = 180 \text{ km s}^{-1}$. The short-dashed line indicates zero rotation in the Galaxy.

$180 < V_{\text{total}} < 210 \text{ km s}^{-1}$ might belong to the thick-disk population. Nevertheless, the remaining high- α halo stars exhibit a well-defined trend that is clearly separated from that of the low- α stars.

5. Discussion

As discussed in detail by Gilmore & Wyse (1998), the near-constancy of $[\alpha/\text{Fe}]$ for the high- α and thick-disk stars suggests that they formed in regions with such a high star formation rate that only Type II SNe contributed to their chemical enrichment up to $[\text{Fe}/\text{H}] \simeq -0.4$. On the other hand, the low- α stars originate in regions with a relatively slow chemical evolution so that Type Ia SNe have started to contribute iron at $[\text{Fe}/\text{H}] \simeq -1.5$ causing $[\alpha/\text{Fe}]$ to decrease toward higher metallicities.

The distinction between the two halo populations is greater for $[\text{Mg}/\text{Fe}]$ than for both $[\text{Ca}/\text{Fe}]$ and $[\text{Ti}/\text{Fe}]$, probably because of different SNe Ia yields. According to Tsujimoto et al. (1995), the relative contributions of SNe Ia to the solar abundances are negligible for Mg, 17% for Si, 25% for Ca, and 57% for Fe.

As discussed by Venn et al. (2004), the yields of the neutron-rich isotopes ^{23}Na and ^{58}Ni from massive stars is controlled by the neutron excess, which depends on the initial heavy-element abundance (Arnett 1971). It would be interesting to investigate in more detail whether these dependences could explain the underabundances of Na and Ni in low- α stars and the correlation seen in Fig. 2.

As seen in the Toomre diagram, the high- α stars show evidence of being more bound to the Galaxy and favoring prograde Galactic orbits, while the low- α stars are less bound with two-thirds of them being on retrograde orbits. This suggests that the high- α population is connected to a dissipative component of the Galaxy that experienced rapid chemical evolution similar to that of the thick disk, whereas the low- α stars were accreted from dwarf galaxies that had lower star formation rates.

Present-day dwarf spheroidal galaxies tend to have even lower values of $[\alpha/\text{Fe}]$, $[\text{Na}/\text{Fe}]$, and $[\text{Ni}/\text{Fe}]$ than the low- α

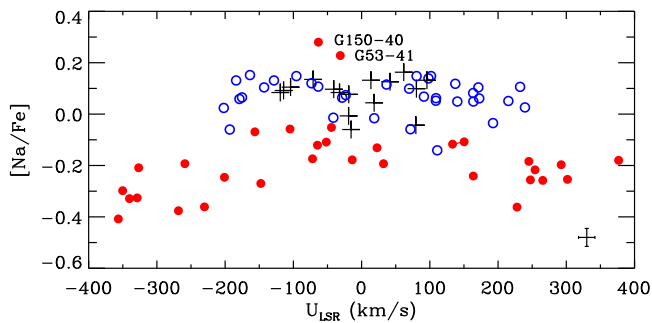


Fig. 4. $[\text{Na}/\text{Fe}]$ versus U_{LSR} for stars with $[\text{Fe}/\text{H}] > -1.4$. The same symbols as in Fig. 3 are used.

halo stars for the range $-1.6 < [\text{Fe}/\text{H}] < -0.8$ (Tolstoy et al. 2009). This offset agrees with the predictions of the simulations of a hierarchically formed stellar halo in a Λ CDM Universe by Font et al. (2006). The bulk of halo stars originate from early accreted, massive dwarf galaxies with efficient star formation, whereas surviving satellite galaxies in the outer halo are on average of lower mass and experience slower chemical evolution with a greater contribution from Type Ia SNe at a given metallicity. The predicted $[\text{Mg}/\text{Fe}]$ versus $[\text{Fe}/\text{H}]$ relation for the accreted halo stars agrees remarkably well with the trend for the low- α halo stars. However, Font et al. do not explain the existence of high- α halo stars. Two Λ CDM simulations suggest a dual origin of stars in the inner Galactic halo. Purcell et al. (2009) propose that ancient stars formed in the Galactic disk may be ejected into the halo by the merging of satellite galaxies, and Zolotov et al. (2009) find that stars formed out of accreted gas in the inner 1 kpc of the Galaxy can be displaced into the halo through a succession of mergers. Alternatively, the high- α population might have formed as the first stars in a dissipative collapse of a proto-Galactic gas cloud (Gilmore et al. 1989; Schuster et al. 2006, Sect. 8.2).

The retrograde low- α stars in Fig. 3 have an average Galactic rotation velocity of $V_{\text{LSR}} \simeq -260 \text{ km s}^{-1}$, which is close to that of the ω Cen globular cluster (Dinescu et al. 1999). As often discussed (e.g., Bekki & Freeman 2003), ω Cen is probably the nucleus of a captured satellite galaxy with its own chemical enrichment history. Meza et al. (2005) simulated the orbital characteristics of the tidal debris of such a satellite dragged into the Galactic plane by dynamical friction. The captured stars have rather small W -velocities but a wide, double-peaked U -distribution, similar to the W - U distribution observed for the low- α halo (see Online Section). As shown in Fig. 4, stars with extreme U velocities tend to have the lowest $[\text{Na}/\text{Fe}]$ values, which corroborates their having a special origin.

In support of a connection between low- α stars and ω Cen, we note that stars in this globular cluster exhibit a wide range of $[\text{Fe}/\text{H}]$ values and a decline in $[\alpha/\text{Fe}]$ for metallicities above $[\text{Fe}/\text{H}] \sim -1$ (Origlia et al. 2003). Johnson et al. (2009), on the other hand, find that $[\text{Na}/\text{Fe}]$ in ω Cen red giants increases from about -0.2 dex at $[\text{Fe}/\text{H}] \sim -1.7$ to $+0.8$ dex at $[\text{Fe}/\text{H}] \sim -1.0$. A similar increase is not seen for the low- α halo stars. Enhancements of Na and a Na-O anticorrelation are present in all well-studied globular clusters (Carretta et al. 2009) and may be caused by the chemical enrichment from intermediate-

mass AGB stars undergoing hot-bottom hydrogen burning. According to the hydrodynamical simulations of D’Ercole et al. (2008), the gas ejected from these AGB stars collects in the cluster core via cooling flows, which may explain the difference in $[\text{Na}/\text{Fe}]$ between stars remaining in ω Cen itself and those originating in the progenitor galaxy.

We conclude that the derived abundance ratios provide clear evidence of two distinct populations of stars that are among the most metal-rich in the Galactic halo. The reason that previous studies have failed to detect this dichotomy may be ascribed to the lower precision of the abundances for less homogeneous samples of stars, and greater focus on metal-poor stars. The high- α stars may be ancient disk or bulge stars ‘heated’ to halo kinematics by merging satellite galaxies or they could be the first stars formed in a dissipative collapse of a proto-Galactic gas cloud. The low- α stars are probably accreted from dwarf galaxies, and some are likely to be associated with the ω Cen progenitor galaxy. Further studies of possible correlations between the abundance ratios and orbital parameters of the stars may help us to clarify the origin of the two populations.

Acknowledgements. We thank the anonymous referee for comments and suggestions, which helped to improve this Letter significantly.

References

- Arnett, W.D. 1971, *ApJ*, 166, 153
- Bekki, K., & Freeman, K.C. 2003, *MNRAS*, 346, L11
- Carollo, D., Beers, T.C., Lee, Y.S. et al. 2007, *Nature*, 450, 1020
- Carretta, E., Bragaglia, A., Gratton, R., & Lucatello, S. 2009, *A&A*, 505, 139
- D’Ercole, A., Vesperini, E., D’Antona F., McMillan S.L.W., & Recchi, S. 2008, *MNRAS*, 391, 825
- Dinescu, D.I., Girard, T.M., & van Altena, W.F. 1999, *AJ*, 117, 1792
- Eggen, O.J., Lynden-Bell, D., & Sandage, A.R. 1962, *ApJ*, 136, 748
- Font, A.S., Johnston, K.V., Bullock, J.S., & Robertson, B.E. 2006, *ApJ*, 638, 585
- Francis, C., & Anderson, E. 2009, *New Astronomy*, 14, 615
- Fulbright, J.P. 2002, *AJ*, 123, 404
- Gilmore, G. & Wyse, R.F.G. 1998, *AJ*, 116, 748
- Gilmore, G., Wyse, R.F.G., & Kuijken, K. 1989, *ARA&A*, 27, 555
- Gratton, R.G., Carretta, E., Desidera, S., et al. 2003, *A&A*, 406, 131
- Gustafsson, B., Edvardsson, B., Eriksson, K., et al. 2008, *A&A*, 486, 951
- Høg, E., Fabricius, C., Makarov, V.V. et al. 2000, *A&A*, 335, L27
- Johnson, C.I., Pilachowski, C.A., Rich, R.M., & Fulbright, J.P. 2009, *ApJ*, 698, 2048
- Johnson, D.R.H. & Soderblom, D.R. 1987, *AJ*, 93, 864
- Kurucz, R.L., Furenlid, I., Brault, J., & Testerman, L. 1984, *Solar Flux Atlas from 296 to 1300 nm*, National Solar Observatory, Sunspot, New Mexico
- Meza, A., Navarro, J.F., Abadi, M.G., & Steinmetz, M. 2005, *MNRAS*, 359, 93
- Nissen, P.E., Chen, Y.Q., Asplund, M., & Pettini, M. 2004, *A&A*, 415, 993
- Nissen, P.E., & Schuster, W.J. 1997, *A&A*, 326, 751
- Origlia, L., Ferraro, F.R., Bellazzini, M., & Pancino, E. 2003, *ApJ*, 591, 916
- Purcell, C.W., Bullock, J.S., & Kazantzidis S. 2009, *arXiv:0910.5481*
- Ramírez, I., & Meléndez, J. 2005, *ApJ*, 626, 465
- Salim, S., & Gould, A. 2003, *ApJ*, 582, 1011
- Schönrich, R., & Binney, J. 2009, *MNRAS*, 399, 1145
- Schuster, W.J., Beers, T.C., Michel, R., Nissen, P.E., & Garía, G. 2004, *A&A*, 422, 527
- Schuster, W.J., Moitinho, A., Márquez, A., Parrao, L., & Covarrubias, E. 2006, *A&A*, 445, 939
- Searle, L. & Zinn, R. 1978, *ApJ*, 225, 357
- Stephens, A., & Boesgaard, A.M. 2002, *AJ*, 123, 1647
- Tolstoy, E., Hill, V., & Tosi, M. 2009, *ARA&A*, 47, 371
- Tsujiimoto, T., Nomoto, K., Yoshii, Y., et al. 1995, *MNRAS*, 277, 945
- van Leeuwen, F. 2007, *Hipparcos, the New Reduction of the Raw Data*, *Astrophys. Space Sci. Library*, vol. 350 (Springer)

Venn, K.A., Irwin, M., Shetrone, M.D., et al. 2004, AJ, 128, 1177
Zolotov, A., Willman, B., Brooks, A.M., et al. 2009, ApJ, 702, 1058

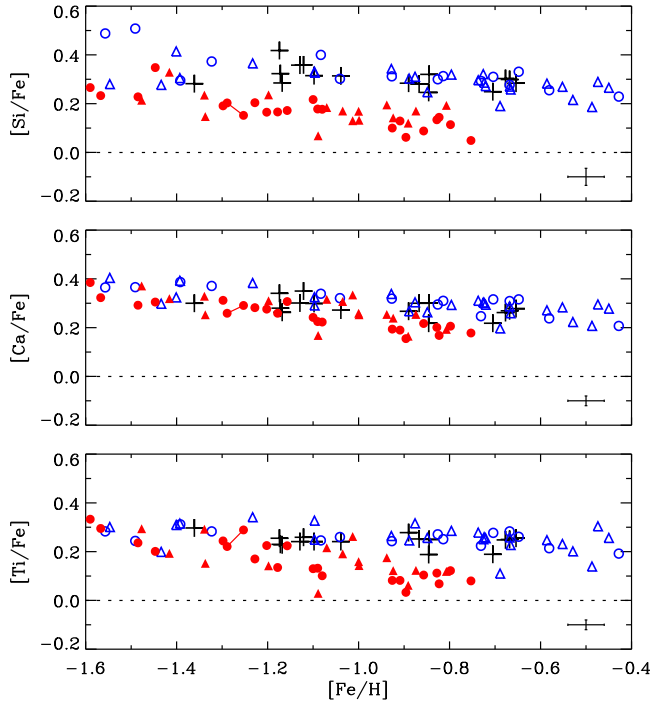


Fig. 5. $[\text{Si}/\text{Fe}]$, $[\text{Ca}/\text{Fe}]$, and $[\text{Ti}/\text{Fe}]$ as a function of $[\text{Fe}/\text{H}]$. The same symbols as in Fig. 1 are used.

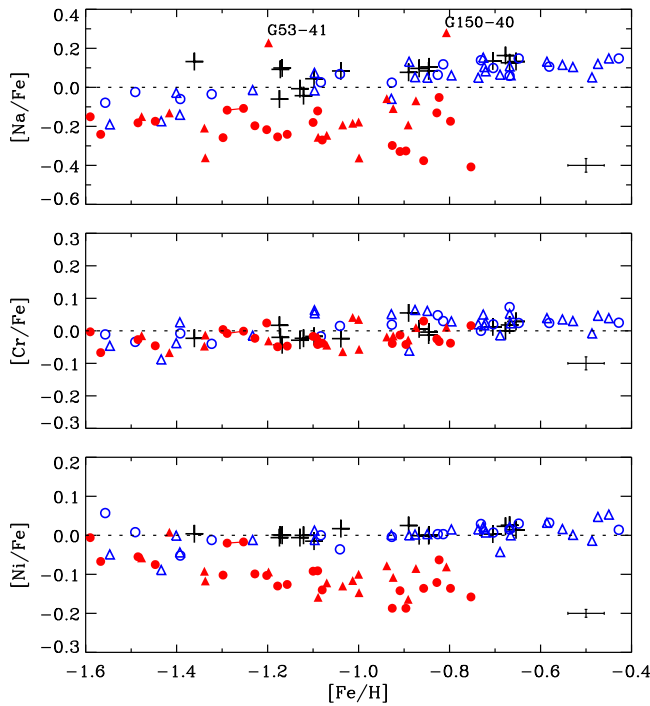


Fig. 6. $[\text{Na}/\text{Fe}]$, $[\text{Cr}/\text{Fe}]$, and $[\text{Ni}/\text{Fe}]$ as a function of $[\text{Fe}/\text{H}]$. The same symbols as in Fig. 1 are used.

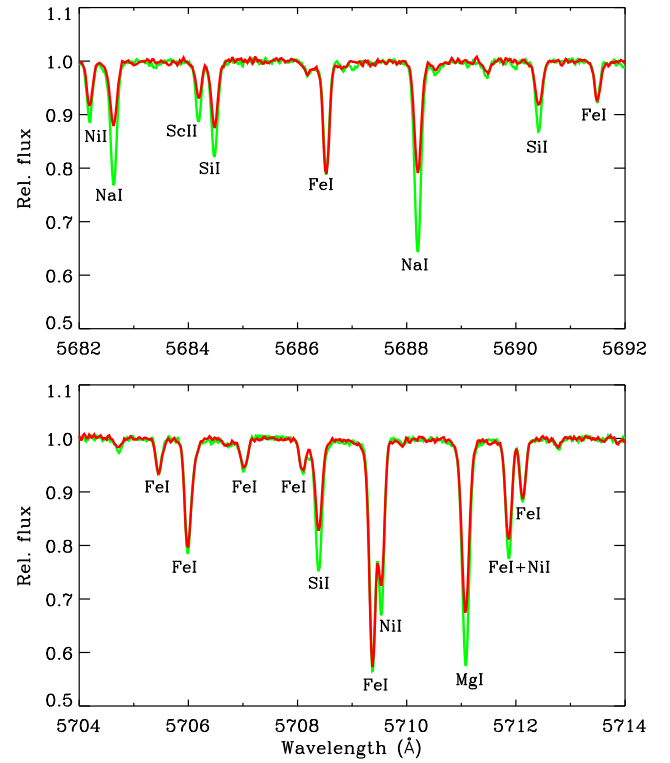


Fig. 7. UVES spectra of two stars with nearly the same atmospheric parameters T_{eff} , $\log g$, and $[\text{Fe}/\text{H}]$. The spectrum of the low- α star CD -45 3283 ($T_{\text{eff}} = 5597$ K, $\log g = 4.55$, $[\text{Fe}/\text{H}] = -0.91$, $[\alpha/\text{Fe}] = 0.12$) is shown with a red line and that of the high- α star G 159-50 ($T_{\text{eff}} = 5624$ K, $\log g = 4.37$, $[\text{Fe}/\text{H}] = -0.93$, $[\alpha/\text{Fe}] = 0.31$) with a green line. The Fe lines have the same strength in the two spectra, but the Na, Mg, Si, and Ni lines are significantly weaker in the spectrum of the low- α star.

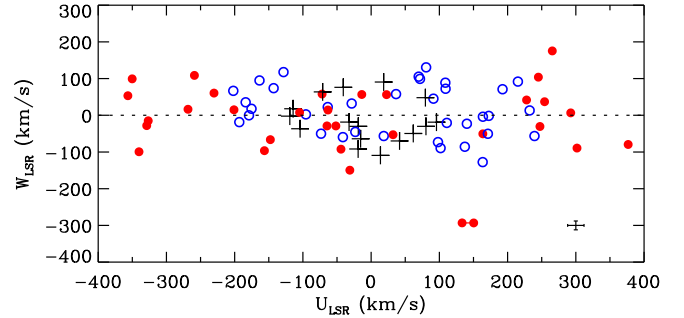


Fig. 8. W_{LSR} versus U_{LSR} for stars with $[\text{Fe}/\text{H}] > -1.4$. The same symbols as in Fig. 3 are used.

Table 1. UVES spectra acquired from the ESO/ST-ECF Science Archive.

ID	Program	Date and UT	S/N	RV ^a (km s ⁻¹)	EW(Na I D ₂) ^b (mÅ)	EW(Na I D ₁) ^b (mÅ)	Note ^c
BD-21 3420	76.B-0133	2006-01-14T08:28	300	7.9	< 3	< 3	
CD-33 3337	68.D-0094	2001-11-26T07:43	600	73.6	< 3	< 3	
CD-43 6810	70.D-0474	2002-12-07T07:58	330	159.2	62	53	
CD-45 3283	69.D-0679	2002-02-19T01:53	300	309.2	< 3	?	
CD-51 4628	69.D-0679	2002-02-18T06:15	280	197.9	15	6	
CD-57 1633	69.D-0679	2002-02-19T01:27	450	260.7	< 3	?	
CD-61 282	76.B-0133	2005-09-22T06:35	280	220.4	?	10 :	
G05-19	76.B-0133	2005-10-15T05:21	300	-216.2	150	130	
G05-40	68.B-0475	2001-10-08T06:25	450	-117.6	196	165	
G18-28	76.B-0133	2005-10-13T00:13	300	-203.1	< 3	< 3	SB1
G18-39	71.B-0529	2003-08-19T07:26	480	-234.1	69	38	
G20-15	71.B-0529	2003-08-11T03:08	500	84.3	198	172	
G46-31	76.B-0133	2005-12-24T03:59	300	220.9	< 3	< 3	SB1
G63-26	72.B-0585	2004-03-23T06:52	240	57.4	29 + 19	19 + 6	
G66-22	69.D-0679	2002-02-18T08:57	250	-145.2	12	6	
G82-05	69.D-0679	2002-02-16T01:22	300	296.0	< 3	< 3	
G112-43	69.D-0679	2002-02-17T02:13	340	-83.7	16	?	
G112-44	70.D-0474	2002-12-31T04:56	350	-84.3	14	7	
G114-42	69.D-0679	2002-02-17T02:58	250	-86.4	64	37	
G121-12	76.B-0133	2006-01-14T07:14	300	197.4	< 3	< 3	
G188-22	71.B-0529	2003-08-09T06:08	450	-93.9	43	18	
G159-50	76.B-0133	2005-10-14T04:17	340	28.0	< 3	< 3	
HD3567	68.B-0475	2001-10-08T04:19	650	-47.8	< 3	< 3	
HD17820	76.B-0133	2005-10-13T06:39	400	6.3	< 3	< 3	
HD22879	68.D-0094	2001-11-26T03:27	450	121.0	< 3	< 3	
HD25704	68.D-0094	2001-11-28T08:24	500	56.0	< 3	< 3	
HD51754	76.B-0133	2005-11-10T08:23	300	-94.0	< 3	< 3	
HD59392	67.D-0086	2001-03-07T03:53	410	268.4	< 3	< 3	
HD76932	67.D-0439	2001-04-10T23:35	600	119.9	< 3	< 3	
HD97320	65.L-0507	2000-04-09T02:09	460	53.5	< 3	< 3	
HD103723	65.L-0507	2000-04-10T02:11	500	168.3	32	18 :	
HD105004	68.B-0475	2002-01-12T07:32	500	121.8	40	21	
HD106516	76.B-0133	2006-01-30T07:04	350	10.6	< 3	< 3	SB1
HD111980	65.L-0507	2000-04-10T03:12	550	159.0	16	?	SB1
HD113679	65.L-0507	2000-04-10T04:39	500	158.0	42 :	?	
HD114762A	77.B-0507	2006-06-08T01:09	475	49.1	< 3	< 3	SB1
HD120559	68.B-0475	2002-02-21T08:17	600	18.6	< 3	< 3	
HD121004	67.D-0439	2001-04-11T05:00	500	244.8	< 3	< 3	
HD126681	65.L-0507	2000-04-09T06:31	500	-45.3	< 3	< 3	
HD132475	65.L-0507	2000-04-12T07:00	500	176.6	28	16	
HD148816	77.B-0507	2006-06-15T03:07	400	-47.8	< 3	< 3	
HD163810	69.D-0679	2002-04-27T08:23	300	185.9	81	72	
HD175179	65.L-0507	2000-04-10T08:46	400	21.9	< 3	< 3	
HD179626	77.B-0507	2006-06-12T06:01	330	-65.0	43	24	
HD189558	65.L-0507	2000-04-09T09:04	600	-12.4	< 3	< 3	
HD193901	77.B-0507	2006-06-12T06:21	380	-171.2	< 3	< 3	
HD194598	77.B-0507	2006-06-25T03:33	270	-247.0	< 3	< 3	
HD199289	77.B-0507	2006-06-04T01:25	290	-5.6	< 3	< 3	
HD205650	65.L-0507	2000-04-12T09:45	480	-105.7	< 3	< 3	
HD219617	77.B-0507	2006-05-29T08:46	370	13.9	< 3	< 3	
HD222766	76.B-0133	2005-10-13T00:44	310	-85.5	< 3	< 3	
HD241253	76.B-0133	2005-10-08T07:52	300	-15.7	< 3	< 3	
HD284248	70.D-0474	2002-12-31T02:50	500	338.9	71	63	

^a Heliocentric radial velocity.^b Equivalent widths of interstellar NaD lines. A question mark means that the line is so badly blended by a stellar or telluric line that it could not be measured.^c Single-lined spectroscopic binaries according to the SIMBAD database are designated with SB1.

Table 2. Stars observed with the NOT/FIES spectrograph.

ID	Program	Date and UT	S/N	RV^a (km s^{-1})	$EW(\text{Na I D}_2)^b$ ($\text{m}\text{\AA}$)	$EW(\text{Na I D}_1)^b$ ($\text{m}\text{\AA}$)	Note ^c
G05-36	38-013	2008-11-30T01:53	170	−9.6	189	164	
G13-38	37-003	2008-05-14T23:55	160	153.4	< 5	< 5	
G15-23	37-003	2008-05-18T23:59	180	−63.6	53	40	
G16-20	37-003	2008-05-15T01:55	185	170.8	131	95	
G20-15 ^d	37-003	2008-05-21T01:39	170	84.3	206	172	
G21-22	37-003	2008-05-16T19:24	160	59.9	94	69	
G24-13	37-003	2008-05-17T04:50	170	99.3	110	89	
G24-25	37-003	2008-05-21T03:12	160	−312.9	?	166	SB1
G31-55	38-013	2008-12-04T20:56	160	−27.9	30	20	
G49-19	38-013	2008-11-30T14:06	180	75.5	63	46	SB1
G53-41	38-013	2008-12-04T05:41	180	88.4	48	28	
G56-30	37-003	2008-05-20T23:48	185	27.9	< 5	< 5	
G56-36	37-003	2008-05-18T21:16	175	99.0	23	17	
G57-07	37-003	2008-05-14T22:27	170	28.6	49	36	
G74-32	38-013	2008-12-04T11:54	140	3.2	?	?	
G75-31	38-013	2008-11-29T23:56	170	57.7	26	14	
G81-02	38-013	2008-12-04T14:21	140	87.9	120	92	
G85-13	38-013	2008-12-02T02:36	160	174.3	< 5	< 5	
G87-13	38-013	2008-12-02T04:33	180	206.6	105 + 94	67 + 48	
G94-49	38-013	2008-12-02T00:30	170	−163.9	< 5	< 5	
G96-20	38-013	2008-12-01T00:39	180	105.7	28 :	12	
G98-53	38-013	2008-12-04T16:18	160	144.7	136	102	
G99-21	38-013	2008-12-03T19:42	140	128.4	< 5	< 5	
G119-64	37-003	2008-05-17T21:08	210	−195.6	< 5	< 5	
G125-13	37-003	2008-05-19T02:49	175	−175.9	28	18	
G127-26	38-013	2008-11-29T19:59	185	−45.7	116	86	
G150-40	37-003	2008-05-17T08:10	170	−50.5	31	14	
G161-73	37-003	2008-05-20T21:56	155	121.2	134	127	
G170-56	37-003	2008-05-18T01:42	180	−239.9	47	27	
G172-61	38-013	2008-11-30T21:43	170	−206.6	< 5	< 5	SB1
G176-53	37-003	2008-05-17T22:24	170	64.9	< 5	< 5	
G180-24	37-003	2008-05-18T01:34	170	−152.0	< 5	< 5	
G187-18	38-013	2008-12-01T19:15	170	−122.4	15	8	
G192-43	38-013	2008-11-30T04:04	180	191.2	49	35	
G232-18	37-003	2008-05-20T04:50	200	−261.2	< 5	< 5	
HD148816 ^d	37-003	2008-05-16T01:33	200	−47.3	< 5	< 5	
HD159482	37-003	2008-05-16T02:02	150	−138.4	< 5	< 5	
HD160693	37-003	2008-05-15T05:11	160	34.5	?	?	
HD177095	37-003	2008-05-19T04:04	160	90.8	< 5	< 5	
HD179626 ^d	37-003	2008-05-20T03:14	170	−64.9	46	27	
HD189558 ^d	37-003	2008-05-21T05:14	350	−12.6	< 5	< 5	
HD193901 ^d	37-003	2008-05-19T05:20	200	−171.2	< 5	< 5	
HD194598 ^d	37-003	2008-05-15T05:33	180	−246.8	< 5	< 5	
HD230409	37-003	2008-05-15T03:54	165	−1.9	< 5	< 5	
HD233511	38-013	2008-12-01T21:48	180	66.2	< 5	< 5	
HD237822	37-003	2008-05-18T22:20	175	−2.3	< 5	< 5	
HD250792A	38-013	2008-12-01T02:17	160	−191.3	< 5	< 5	

^a Heliocentric radial velocity.^b Equivalent widths of interstellar NaD lines. A question mark means that the line is so badly blended by a stellar or telluric line that it could not be measured.^c Single-lined spectroscopic binaries according to the SIMBAD database are designated with SB1.^d UVES spectrum is also available.

Table 3. Atmospheric parameters, abundance ratios, and space velocities for stars with VLT/UVES spectra.

ID	T_{eff} (K)	$\log g$	$[\frac{\text{Fe}}{\text{H}}]$	ξ_{turb} (km/s)	$[\frac{\text{Na}}{\text{Fe}}]$	$[\frac{\text{Mg}}{\text{Fe}}]$	$[\frac{\text{Si}}{\text{Fe}}]$	$[\frac{\text{Ca}}{\text{Fe}}]$	$[\frac{\text{Ti}}{\text{Fe}}]$	$[\frac{\text{Cr}}{\text{Fe}}]$	$[\frac{\text{Ni}}{\text{Fe}}]$	U_{LSR} (km/s)	V_{LSR} (km/s)	W_{LSR} (km/s)	Class ^a
BD-21 3420	5808	4.26	-1.13	1.3	-0.01	0.32	0.36	0.30	0.24	-0.03	-0.01	-19	-87	-92	TD
CD-33 3337	5979	3.86	-1.36	1.7	0.13	0.32	0.28	0.30	0.30	-0.02	0.00	14	-42	-109	TD
CD-43 6810	5945	4.26	-0.43	1.3	0.15	0.28	0.23	0.21	0.19	0.03	0.01	102	-159	-89	high- α
CD-45 3283	5597	4.55	-0.91	1.0	-0.33	0.08	0.13	0.19	0.08	-0.01	-0.14	-340	-213	-99	low- α
CD-51 4628	6153	4.31	-1.30	1.4	-0.26	0.13	0.19	0.31	0.24	0.00	-0.10	266	-129	175	low- α
CD-57 1633	5873	4.28	-0.90	1.2	-0.33	0.03	0.06	0.16	0.03	-0.04	-0.19	-329	-240	-28	low- α
CD-61 282	5759	4.31	-1.23	1.3	-0.20	0.21	0.20	0.28	0.17	-0.02	-0.10	293	-284	7	low- α
G05-19	5854	4.26	-1.18	1.3	-0.25	0.18	0.17	0.26	0.14	-0.05	-0.13	302	-274	-89	low- α
G05-40	5795	4.17	-0.81	1.2	0.12	0.35	0.31	0.31	0.25	0.03	0.00	137	-218	-86	high- α
G18-28	5372	4.41	-0.83	1.0	0.06	0.36	0.30	0.29	0.27	0.05	0.00	-29	-214	32	high- α
G18-39	6040	4.21	-1.39	1.5	-0.06	0.35	0.29	0.39	0.31	-0.01	-0.05	-193	-257	-19	high- α
G20-15	6027	4.32	-1.49	1.6	-0.18	0.22	0.23	0.29	0.24	-0.03	-0.05	161	-60	-210	(low- α)
G46-31	5901	4.23	-0.83	1.4	-0.13	0.15	0.13	0.20	0.11	-0.03	-0.12	23	-310	56	low- α
G63-26	6043	4.18	-1.56	1.8	-0.08	0.35	0.49	0.37	0.28	-0.01	0.06	90	-332	43	(high- α)
G66-22	5236	4.41	-0.86	0.9	-0.38	0.08	0.09	0.22	0.10	0.03	-0.14	-268	-191	16	low- α
G82-05	5277	4.45	-0.75	0.9	-0.41	0.06	0.05	0.18	0.08	0.02	-0.16	-357	-180	53	low- α
G112-43	6074	4.03	-1.25	1.3	-0.11	0.21	0.15	0.29	0.29	0.00	-0.02	145	-119	-293	low- α
G112-44	5819	4.25	-1.29	1.2	-0.12	0.22	0.20	0.26	0.22	-0.01	-0.02	138	-109	-293	low- α
G114-42	5643	4.38	-1.10	1.3	-0.18	0.18	0.22	0.24	0.13	-0.02	-0.09	377	-189	-80	low- α
G121-12	5928	4.23	-0.93	1.4	-0.30	0.03	0.10	0.19	0.08	-0.04	-0.19	-350	-202	99	low- α
G188-22	5974	4.18	-1.32	1.5	-0.04	0.39	0.37	0.37	0.28	-0.04	-0.01	193	-99	71	high- α
G159-50	5624	4.37	-0.93	1.1	0.02	0.38	0.31	0.32	0.24	0.02	0.00	-202	-192	67	high- α
HD3567	6051	4.02	-1.16	1.5	-0.24	0.14	0.17	0.31	0.22	-0.05	-0.13	164	-259	-51	low- α
HD17820	5773	4.22	-0.67	1.3	0.13	0.35	0.30	0.27	0.25	0.02	0.03	42	-85	-70	TD
HD22879	5759	4.25	-0.85	1.3	0.10	0.36	0.32	0.30	0.25	0.00	0.00	-104	-76	-37	TD
HD25704	5868	4.26	-0.85	1.4	0.08	0.32	0.25	0.22	0.19	-0.01	0.00	-119	-53	-2	TD
HD51754	5767	4.29	-0.58	1.4	0.11	0.33	0.25	0.24	0.21	0.02	0.03	232	-150	13	high- α
HD59392	6012	3.91	-1.60	1.9	-0.15	0.28	0.27	0.38	0.33	0.00	-0.01	115	-307	-25	(low- α)
HD76932	5877	4.13	-0.87	1.4	0.10	0.34	0.28	0.30	0.25	0.01	0.00	-41	-77	76	TD
HD97320	6008	4.19	-1.17	1.6	0.10	0.34	0.28	0.26	0.23	-0.04	0.00	80	-11	-30	TD
HD103723	5938	4.19	-0.80	1.2	-0.17	0.10	0.11	0.21	0.12	-0.04	-0.14	-72	-193	58	low- α
HD105004	5754	4.30	-0.82	1.2	-0.05	0.17	0.14	0.17	0.07	-0.03	-0.06	-44	-239	-92	low- α
HD106516	6196	4.42	-0.68	1.3	0.16	0.34	0.30	0.26	0.25	0.00	0.02	62	-61	-50	TD
HD111980	5778	3.96	-1.08	1.5	0.03	0.36	0.40	0.34	0.25	-0.02	0.00	239	-174	-57	high- α
HD113679	5672	3.99	-0.65	1.4	0.15	0.37	0.33	0.32	0.26	0.02	0.03	-96	-278	3	high- α
HD114762A	5856	4.21	-0.70	1.5	0.14	0.29	0.25	0.22	0.19	0.01	0.00	-71	-53	64	TD
HD120559	5412	4.50	-0.89	1.1	0.08	0.36	0.28	0.27	0.28	0.05	0.03	-19	-38	-30	TD
HD121004	5669	4.37	-0.70	1.3	0.10	0.36	0.31	0.32	0.28	0.02	0.01	70	-242	105	high- α
HD126681	5507	4.45	-1.17	1.2	-0.06	0.38	0.42	0.34	0.25	0.02	-0.01	-15	-28	-64	TD
HD132475	5646	3.76	-1.49	1.5	-0.02	0.41	0.51	0.37	0.24	-0.03	0.01	44	-371	60	(high- α)
HD148816	5823	4.13	-0.73	1.4	0.14	0.32	0.29	0.25	0.22	0.00	0.03	98	-260	-73	high- α
HD163810	5501	4.56	-1.20	1.3	-0.22	0.18	0.17	0.28	0.22	0.02	-0.10	254	-193	37	low- α
HD175179	5713	4.33	-0.65	1.2	0.13	0.34	0.28	0.28	0.25	0.03	0.01	96	-102	-19	TD
HD179626	5850	4.13	-1.04	1.6	0.07	0.35	0.30	0.32	0.26	0.01	-0.04	91	-215	45	high- α
HD189558	5617	3.80	-1.12	1.4	-0.04	0.36	0.36	0.35	0.26	-0.02	0.00	80	-109	48	TD
HD193901	5656	4.36	-1.09	1.3	-0.27	0.13	0.18	0.23	0.11	-0.04	-0.14	-148	-233	-66	low- α
HD194598	5942	4.33	-1.09	1.4	-0.12	0.18	0.18	0.22	0.13	-0.04	-0.09	-65	-267	-29	low- α
HD199289	5810	4.28	-1.04	1.3	0.08	0.36	0.31	0.27	0.24	-0.02	0.02	-32	-55	-19	TD
HD205650	5698	4.32	-1.17	1.3	0.09	0.36	0.32	0.28	0.23	-0.02	0.00	-114	-71	18	TD
HD219617	5862	4.28	-1.45	1.5	-0.17	0.26	0.35	0.31	0.20	-0.05	-0.08	228	-174	-32	(low- α)
HD222766	5334	4.27	-0.67	0.8	0.06	0.35	0.28	0.31	0.28	0.07	0.01	-179	-173	0	high- α
HD241253	5831	4.31	-1.10	1.3	0.04	0.32	0.31	0.30	0.24	-0.02	-0.01	18	-74	91	TD
HD284248	6135	4.25	-1.57	1.6	-0.24	0.22	0.23	0.32	0.29	-0.07	-0.07	-349	-150	-70	(low- α)

^a Classification as thick disk (TD), low- α , or high- α . For halo stars with $[\text{Fe}/\text{H}] < -1.4$, the classification is uncertain and given in parentheses.

Table 4. Atmospheric parameters, abundance ratios, and space velocities for stars with NOT/FIES spectra.

ID	T_{eff} (K)	$\log g$	$[\text{Fe}/\text{H}]$	ξ_{turb} (km/s)	$[\text{Na}/\text{Fe}]$	$[\text{Mg}/\text{Fe}]$	$[\text{Si}/\text{Fe}]$	$[\text{Ca}/\text{Fe}]$	$[\text{Ti}/\text{Fe}]$	$[\text{Cr}/\text{Fe}]$	$[\text{Ni}/\text{Fe}]$	U_{LSR} (km/s)	V_{LSR} (km/s)	W_{LSR} (km/s)	Class ^a
G05-36	6013	4.23	-1.23	1.4	-0.01	0.33	0.37	0.38	0.34	-0.01	-0.01	-41	-297	-60	high- α
G13-38	5263	4.54	-0.88	0.9	0.05	0.35	0.31	0.30	0.32	0.06	0.00	109	-143	89	high- α
G15-23	5297	4.57	-1.10	1.0	-0.02	0.40	0.33	0.32	0.33	0.06	-0.01	19	-176	-57	high- α
G16-20	5625	3.64	-1.42	1.5	-0.13	0.22	0.33	0.32	0.19	-0.07	0.01	208	-143	75	(low- α)
G20-15 ^b	6072	4.36	-1.41	1.1	-0.23	0.20	0.15	0.25	0.22	-0.03	-0.05	161	-60	-210	(low- α)
G21-22	5901	4.24	-1.09	1.4	-0.26	0.09	0.07	0.17	0.03	-0.02	-0.16	247	-258	-31	low- α
G24-13	5673	4.31	-0.72	1.0	0.08	0.34	0.27	0.29	0.25	0.02	0.01	164	-38	-128	high- α
G24-25	5828	3.86	-1.40	1.2	-0.03	0.34	0.41	0.32	0.31	-0.04	0.00	-197	-242	43	(high- α)
G31-55	5638	4.30	-1.10	1.4	0.07	0.28	0.33	0.29	0.25	0.05	0.01	-23	-184	-45	high- α
G49-19	5772	4.25	-0.55	1.2	0.12	0.30	0.27	0.28	0.23	0.04	0.02	37	-236	58	high- α
G53-41	5859	4.27	-1.20	1.3	0.23	0.24	0.24	0.31	0.14	-0.03	-0.09	-31	-299	-150	low- α
G56-30	5830	4.26	-0.89	1.3	-0.19	0.10	0.12	0.17	0.06	-0.03	-0.16	32	-283	-53	low- α
G56-36	5933	4.28	-0.94	1.4	-0.06	0.19	0.19	0.25	0.17	-0.02	-0.08	-105	-247	8	low- α
G57-07	5676	4.25	-0.47	1.1	0.12	0.34	0.29	0.29	0.30	0.05	0.05	-73	-162	-50	high- α
G74-32	5772	4.36	-0.72	1.1	0.10	0.37	0.29	0.30	0.26	0.02	0.02	-143	-151	74	high- α
G75-31	6010	4.02	-1.03	1.4	-0.19	0.12	0.17	0.31	0.19	-0.06	-0.13	-259	-206	109	low- α
G81-02	5859	4.19	-0.69	1.3	0.06	0.25	0.19	0.20	0.11	-0.01	-0.04	-175	-201	18	high- α
G85-13	5628	4.38	-0.59	1.0	0.13	0.33	0.28	0.27	0.25	0.04	0.03	-184	-43	35	high- α
G87-13	6085	4.13	-1.09	1.5	-0.25	0.10	0.18	0.32	0.22	-0.04	-0.12	-201	-286	15	low- α
G94-49	5373	4.50	-0.80	1.1	0.06	0.34	0.32	0.29	0.28	0.03	0.01	172	-96	-2	high- α
G96-20	6293	4.41	-0.89	1.5	0.13	0.30	0.30	0.27	0.25	-0.06	0.00	-128	-91	118	high- α
G98-53	5848	4.23	-0.87	1.3	-0.07	0.20	0.17	0.25	0.12	0.01	-0.09	-156	-263	-96	low- α
G99-21	5487	4.39	-0.67	0.9	0.11	0.33	0.27	0.29	0.26	0.05	0.02	-64	-182	22	high- α
G119-64	6181	4.18	-1.48	1.5	-0.15	0.25	0.21	0.37	0.29	-0.01	-0.06	237	-291	-120	(low- α)
G125-13	5848	4.28	-1.43	1.5	-0.17	0.30	0.28	0.30	0.20	-0.09	-0.09	215	-228	-157	(high- α)
G127-26	5791	4.14	-0.53	1.2	0.10	0.31	0.22	0.22	0.20	0.03	0.00	171	-83	-50	high- α
G150-40	5968	4.09	-0.81	1.4	0.28	0.14	0.19	0.19	0.12	0.01	-0.08	-63	-318	14	low- α
G161-73	5986	4.00	-1.00	1.4	-0.36	0.13	0.13	0.25	0.14	-0.06	-0.15	228	-250	42	low- α
G170-56	5994	4.12	-0.92	1.5	-0.11	0.17	0.14	0.24	0.12	-0.02	-0.11	-52	-289	-29	low- α
G172-61	5225	4.47	-1.00	0.9	-0.18	0.16	0.17	0.26	0.16	0.04	-0.10	-14	-267	57	low- α
G176-53	5523	4.48	-1.34	1.0	-0.36	0.15	0.15	0.25	0.15	-0.01	-0.12	-230	-271	61	low- α
G180-24	6004	4.21	-1.39	1.5	-0.14	0.31	0.31	0.39	0.31	0.03	-0.04	111	-245	-21	high- α
G187-18	5607	4.39	-0.67	1.1	0.06	0.29	0.26	0.26	0.23	0.02	0.00	109	-130	72	high- α
G192-43	6170	4.29	-1.34	1.5	-0.21	0.19	0.23	0.33	0.29	-0.05	-0.09	-327	-224	-15	low- α
G232-18	5559	4.48	-0.93	1.3	-0.06	0.35	0.34	0.34	0.26	0.05	0.00	72	-242	99	high- α
HD148816 ^b	5840	4.14	-0.70	1.4	0.14	0.32	0.27	0.26	0.20	0.02	0.02	98	-260	-73	high- α
HD159482	5737	4.31	-0.73	1.3	0.15	0.34	0.32	0.30	0.25	0.05	0.02	-164	-47	95	high- α
HD160693	5714	4.27	-0.49	1.1	0.05	0.24	0.19	0.21	0.14	-0.01	-0.01	215	-105	92	high- α
HD177095	5349	4.39	-0.74	0.9	0.05	0.38	0.30	0.31	0.28	0.02	0.01	140	-138	-23	high- α
HD179626 ^b	5855	4.19	-1.00	1.4	0.06	0.36	0.32	0.34	0.26	0.03	-0.05	91	-215	45	high- α
HD189558 ^b	5623	3.81	-1.12	1.4	-0.01	0.38	0.38	0.36	0.27	-0.01	0.01	80	-109	48	TD
HD193901 ^b	5676	4.41	-1.07	1.4	-0.30	0.17	0.16	0.23	0.11	-0.04	-0.14	-148	-233	-66	low- α
HD194598 ^b	5926	4.32	-1.08	1.4	-0.10	0.23	0.21	0.22	0.14	-0.03	-0.09	-65	-267	-29	low- α
HD230409	5318	4.54	-0.85	1.1	0.05	0.30	0.25	0.26	0.26	0.06	0.00	164	-114	-4	high- α
HD233511	6006	4.23	-1.55	1.3	-0.19	0.36	0.28	0.40	0.30	-0.05	-0.05	-131	-243	31	(high- α)
HD237822	5603	4.33	-0.45	1.1	0.15	0.35	0.26	0.28	0.26	0.04	0.05	81	-131	131	high- α
HD250792A	5489	4.47	-1.01	1.1	-0.18	0.23	0.13	0.33	0.26	0.04	-0.12	245	-237	104	low- α

^a Classification as thick disk (TD), low- α , or high- α . For halo stars with $[\text{Fe}/\text{H}] < -1.4$, the classification is uncertain and given in parentheses.^b Data are also available from UVES spectra (see Table 3). In the figures, abundance data based on the UVES spectra are plotted.